Diamond & Related Materials 19 (2010) 368–373

Contents lists available at ScienceDirect

Diamond & Related Materials

journal homepage: www.elsevier.com/locate/diamond

The ultimate diamond slab: GraphAne versus graphEne

Enrique Muñoz [1], Abhishek K. Singh, Morgana A. Ribas, Evgeni S. Penev, Boris I. Yakobson *

Department of Mechanical Engineering and Materials Science, Rice University, Houston TX 77005, USA
Department of Chemistry, Rice University, Houston TX 77005, USA
Richard Smalley Institute for Nanoscale Science and Technology, Rice University, Houston TX 77005, USA

ARTICLE INFO

Available online 13 January 2010

Keywords:
Diamond
Graphene
Nano-mechanics
Electronics
Thermal transport

ABSTRACT

In this article, we present a comprehensive characterization of three carbon nanomaterials of technological interest: graphene, graphane, and fluorinated graphene. By means of first principles and tight-binding calculations in combination with analytical methods, we carried out detailed comparative studies of their structural, mechanical, thermal, and electronic properties. The calculated elastic properties of these materials confirm their high mechanical stability and stiffness, which in association with their low dimensionality, translates into a large ballistic thermal conductance. Furthermore, we show that while graphene is a zero gap semi-metal, graphane and fluorinated graphene are wide gap semiconductors. Finally, we discuss designed interfaces between these systems, and show that their physical properties have potential applications in nanoelectronic devices.

1. Introduction

In the recent studies of hydrogen storage, a catalytic process called *spillover* has emerged as one of the promising methods (see [1,2] and references therein). Through our modeling of the spillover onto graphitic substrate-receptors, we came to realize that hydrogenation must proceed as a new phase nucleation [2], in order to make the process thermodynamically feasible. Indeed, while an individual H binds to the sp^2-carbon rather weakly (below its binding within molecular H_2), an island of tens of H-atoms densely covering the graphene-receptor on both sides appears more favorable than the molecular gas phase, at nearly ambient conditions. Such CH-islands of previously predicted graphane [3] should form sharp interfaces with the initially pristine graphene [1,2,4]. Combining these two distinctly different materials within the same two-dimensional layout [4,5] offers interesting opportunities for nanoengineering and possibly device functionality.

Graphene, a two-dimensional array of carbon atoms in a honeycomb lattice, can be considered as a single monolayer of graphite. It was synthesized by mechanical exfoliation of graphite for the first time in 2004 [6,7]. Its singular electronic spectrum, which displays a linear dispersion near the Fermi point, has been the recent focus of attention for many theoretical and experimental studies, particularly as a solid-state model for Dirac's equation [8]. In addition, being a quasi-two-dimensional object, graphene exhibits a nearly ballistic mechanism for charge and energy transport at the nanometer scale. Mechanical properties of graphene are also remarkable, with the largest Young modulus experimentally measured for any material [9]. Possessing a carbon framework similar to graphene, graphane is an extended two-dimensional and covalently bonded hydrocarbon [3]. Hydrogenation in graphane induces a change in carbon hybridization from sp^2 to sp^3, thus leading to a non-planar structure [3]. Therefore, graphane may be considered as a slab of diamond reduced to its ultimately thin monoatomic version. This similarity to diamond makes it understandable that the hydrogenation also changes the electronic band structure in graphane with respect to graphene, the former being a wide gap semiconductor [3]. Interestingly, before graphane was theoretically postulated as a stable material, graphite derived carbon structures by fluorination were discovered experimentally [10–12]. Of particular interest in this context is fluorinated graphene, structurally similar to graphane.

In this article, we present theoretical estimations for the physical properties of graphene, graphane, and fluorinated graphene. By means of *ab initio* calculations and analytical methods, we will compare mechanical, thermal, and electronic properties of these carbon nanomaterials. In addition, we will discuss designed interfaces between these systems, and their potential applications [4] in nanodevices.

2. Structural stability and nanomechanics

First, we present *ab initio* calculations for the structures and mechanical properties of graphene, graphane, and fluorinated graphene. Following the approach in Refs. [13,14], we approximate the mechanical response of these two-dimensional atomic lattices by an isotropic, continuum elastic shell model. This simplification is well justified for the hexagonal graphene lattice, which possesses isotropic

* Corresponding author.
E-mail address: biy@rice.edu (B.I. Yakobson).
[1] *Present address*: Departamento de Matematica y Fisica, Universidad de Playa Ancha, Avda. Leopoldo Carvallo 270, Playa Ancha, Valparaíso, Chile.

0925-9635/$ – see front matter © 2010 Elsevier B.V. All rights reserved.
doi:10.1016/j.diamond.2010.01.007

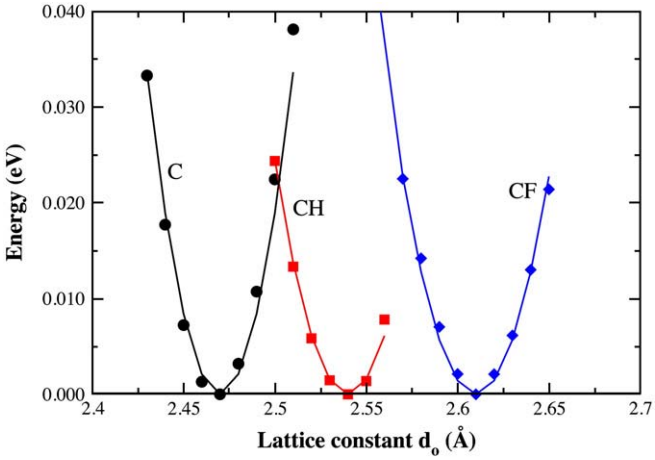

Fig. 1. Calculated elastic energies as a function of the lattice parameter. The values are reported on a per unit cell basis (stoichiometries: graphene C, graphane CH, and fluorinated graphene CF), and measured with respect to the equilibrium configuration. Also shown are quadratic fits for the three materials.

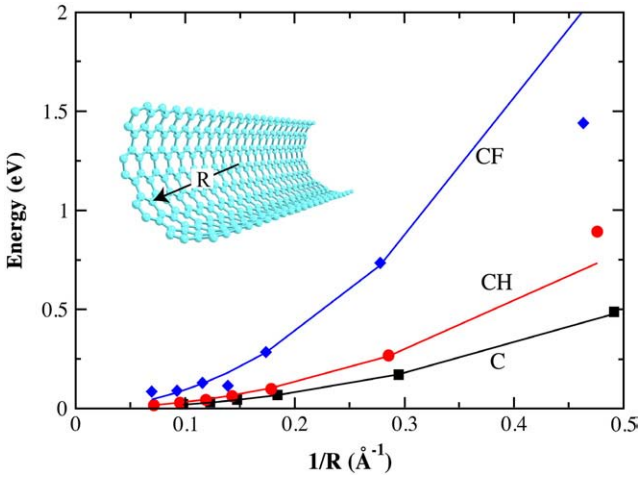

Fig. 2. Calculated elastic energies as a function of the curvature, for tubes of different radii. The values are reported on a per carbon atom basis, and measured with respect to the flat geometry. Also shown are quadratic fits for the three materials.

elastic properties [14,15]. The assumption of isotropy in non-planar lattices such as graphane and fluorinated graphene, where the symmetry group is reduced from $D_{6\,h}$ to $P\bar{3}m1$ (in chair configuration), cannot be rigorously justified from an atomistic point of view, but will be still taken as a reasonable approximation at a mesoscopic scale. We calculate the in-plane rigidity C, defined as the elastic energy required to stretch a single sheet of material, by fitting a parabola to the energy per carbon atom $U = (1/2)\tilde{C}\epsilon^2$. Here, $\epsilon = (d - d_0)/d_0$ is the strain normalized with respect to the equilibrium lattice parameter. The in-plane rigidity is obtained from the coefficient in the fit by $C = \tilde{C}/d_0^2$. The total energies are calculated using density functional theory with plane-wave basis set and projected augmented wave type pseudopotential as implemented in VASP [16–20]. The exchange and correlation part of the energy are approximated by PBE functional [21]. The calculated energy per unit cell, as a function of the lattice parameter, is shown in Fig. 1 for graphene, graphane, and fluorinated graphene, respectively. The equilibrium lattice parameters, 2.8% greater for graphane (CH) and almost 5% greater for fluorinated graphene (CF) (both relative to graphene) indicate significant mismatch for possible interfaces of interest, discussed later in the paper. The resulting ±1.5% strain may also cause rumpling of graphane at the intermediate stages of its formation. The in-plane stiffness obtained from these calculations for the three materials is shown in Table 1.

We also estimated the bending stiffness of graphene, graphane, and fluorinated graphene, by defining the elastic energy due to curvature as $U = (1/2)\tilde{D}/R^2$. The bending stiffness D is obtained from the coefficient in the parabolic fit through the relation $D = \tilde{D}/A$, where $A = \sqrt{3}d_0^2/4$ is the area per carbon atom in a hexagonal array, and d_0 is the equilibrium lattice constant as given in Table 1. For that purpose, we obtained the total energy per carbon atom of pristine, hydrogenated, and fluorinated nanotubes of different radii. We used a density functional based tight-binding method, implemented in the DFTB+ code [22,23]. As shown in Fig. 2, the energy approximately follows a parabola as a function of curvature $1/R$. Hydrogenated tubes, corresponding to curved graphane, show a positive deviation from the parabolic relation at small radii. This feature can be explained to be a consequence of steric effects associated to the close proximity between hydrogen groups in the lumen of very small tubes, which induces an effective repulsive interaction. A deviation on the opposite sense is observed in fluorinated graphene, since in small tubes internal fluorinated groups attract each other. This tendency is observed also in linear fluorinated hydrocarbons, and is usually called the Gauche effect in this context [24].

Table 1
Calculated mechanical properties of graphene, graphane and fluorinated graphene.

Material	d_0 (Å)	ρ_s (mg/m^2)	C (N/m)	D (eV)	h (Å)	Y (Pa)
Graphene	2.47	0.755	352.54	1.48	0.85	4.63E + 12
Graphane	2.54	0.773	244.95	2.18	1.32	1.84E + 12
F-graphene	2.61	1.746	227.80	6.34	2.29	1.01E + 12

From the calculations of the well defined in-plane and bending stiffness, one can estimate two properties which have no direct definition at the nearly two-dimensional atomistic level: the effective thickness h of the sheet, and the Young modulus Y. In agreement with Ref. [13], we define these properties by means of the expressions from an equivalent continuum elastic shell model, $D = Yh^3/12(1-\nu^2)$, and $C = Yh$. By combining these two relations, we obtain an unambiguous definition of Y and h. The relaxed structures of CH and CF nanotubes are shown in Fig. 3. A summary of the calculated properties for all three materials is presented in Table 1. According to these results, graphene is the most rigid among the three materials upon stretching, but the most compliant upon bending. In graphane and fluorinated graphene, the sp^3 carbon hybridization induces non-planar structures. This effect, in combination with interactions between the surface CF or CH groups, translates into a higher bending stiffness and a larger effective thickness.

3. Ballistic thermal conductance

The characterization of basic elastic parameters above, such as in-plane rigidity and bending stiffness, allows one to estimate general features of the vibrational dynamics as well: frequencies, speed of sound and phonon density of states. At reasonably low temperatures, the phonon spectrum is dominated by long wavelength acoustic modes, which can be described from a continuum shell model. A particularly relevant application of this analysis is the estimation of thermal transport properties in nanostructures. Since graphite, a crystalline form of carbon, exhibits a high thermal conductivity at room temperature (~2000 W/m/K), it is believed that low-dimensional forms of this material, such as carbon nanotubes and graphene sheets, may share or even exceed this value. Molecular dynamics (MD) simulations [25] once suggested that thermal conductivity in carbon nanotubes may be as high as 6000 W/m/K. Other MD results reported thermal conductivities of about 2000 W/m/K for carbon nanotubes [26], and even higher values for single-layer graphene [26]. Recently, experimental measurements were reported [27] on

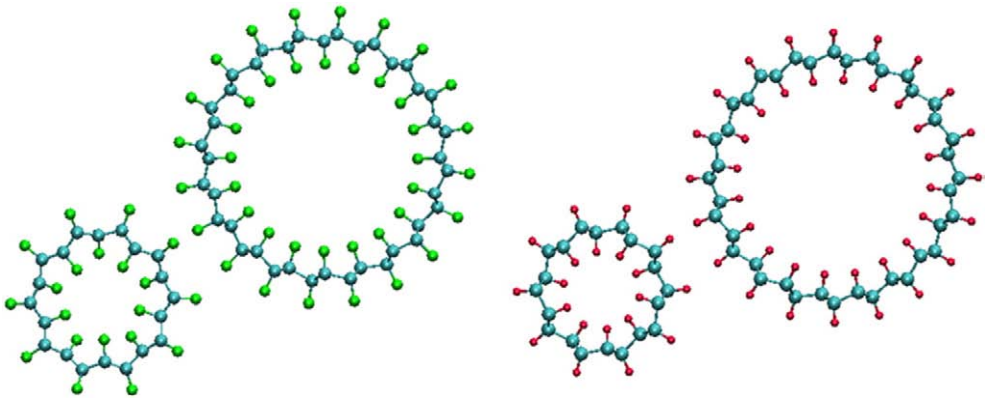

Fig. 3. Relaxed structures for fluorinated graphene (left) and graphane (right) tubes. A single unit cell is displayed, for armchair edges (n,n) with $n=10$ and $n=5$, respectively.

graphene sheets of ~10 μm length, with thermal conductivities in the range of 3080–5150 W/m/K at room temperature. These extremely high values can be explained by the large phonon mean free path in nanostructures such as carbon nanotubes [28] and graphene sheets [27], which can typically exceed 500 nm. Therefore, it is theoretically expected that thermal conductivity at the nanoscale is dominated by a ballistic mechanism. Based on phonon spectra obtained from an atomistic description of graphene, independent estimations for the ballistic thermal conductance of a single graphene layer have been reported in the literature [29,30]. In particular, a low-temperature dependence $\sim T^{1.5}$ was obtained for an infinite graphene sheet [29,30].

Recently, we obtained an analytical expression to calculate the ballistic thermal conductance per unit width of thin ribbons [31]. In our theory, we approximate the phonon spectra of the graphene sheet by using a model from continuum elasticity [31]. Let us consider an elastic ribbon with a finite width w, and assume the length $L\to\infty$. In this situation, points in the reciprocal space are discrete in the transverse direction-y, but constitute a quasi-continuum in the longitudinal direction-x. We thus have $\vec{k}=(k_x, 2\pi n_y/L)$, with integers $-(N_y-1)/2\le n_y\le(N_y-1)/2$. Here, N_y represents the total number of modes to be included in correspondence with the total number of unit cells in the y-direction, for an equivalent atomic lattice system. The vibration frequencies for a thin ribbon with finite width w, and infinite length $L\to\infty$ are given by [31]:

$$\begin{aligned}\text{Bending}: \omega_b = c_b\left|\vec{k}\right|^2,\ \text{LA}: \omega_{\text{LA}} = c_{\text{LA}}\left|\vec{k}\right|,\ \text{TA}\\ : \omega_{\text{TA}} = c_{\text{TA}}\left|\vec{k}\right|,\ \text{Torsion}: \omega_\tau = c_\tau k_x.\end{aligned} \quad (1)$$

Here, we have defined the coefficients $c_b=\sqrt{D/\rho_s}$, $c_{\text{LA}}=\sqrt{C/\rho_s(1-\nu^2)}$, $c_{\text{TA}}=\sqrt{C/2\rho_s(1+\nu)}$, and $c_\tau=(1/w)\sqrt{8(1-\nu)D/\rho_s}$ [31]. Due to the quadratic dispersion of the bending mode, the coefficient c_b does not possess dimensions of velocity, in contrast with the remaining ones representing the speed of sound in the LA, TA, and torsion modes, respectively. The speed of sound in the torsion mode vanishes in the limit of a very wide ribbon, $c_\tau \sim 1/w$. The continuum elasticity parameters in this mechanical model are the in-plane rigidity C, the flexural rigidity D, the Poisson ratio ν, and the surface mass density $\rho_s=mN/(Lw)$, as defined in the previous section. To apply our analytical equations for graphene, graphane, and fluorinated graphene, we will use the set of continuum elastic parameters obtained from our calculations as shown in Table 1.

In the spirit of Debye model, we introduce a cutoff in the x-wave number $|k_x|\le k_c$, in order to satisfy the correct number of degrees of freedom $3N-6\sim 3N$, $k_c=\pi n_s^{1/2}$ [31]. Here, $n_s=N/(wL)$ is the surface number density.

With these considerations, an analytical expression for the ballistic thermal conductance of a nano-ribbon is [31]:

$$\begin{aligned}\sigma = \left(k_B^2T/h\right)\sum_{j=b,\text{LA},\text{TA},\tau} f_2\left(\theta_j/T\right) + 2\left(k_B^2T/h\right)\sum_{n_y=1}^{(N_y-1)/2}\left\{\sum_{j=\text{LA},\text{TA}}\left[f_2\left(\theta_j\sqrt{1+4n_y^2/N_y^2}/T\right)\right.\right.\\ \left.\left.-f_2\left(\theta_j 2n_y/\left(N_yT\right)\right)\right] + f_2\left(\theta_b\left[1+4n_y^2/N_y^2\right]/T\right) - f_2\left(4\theta_b n_y^2/\left(N_y^2T\right)\right)\right\}.\end{aligned} \quad (2)$$

This constitutes the main result of our analysis, where the function $f_2(y)=\int_0^y dx x^2e^x/(e^x-1)^2$ and the characteristic temperatures for each mode are: $\theta_b=\hbar c_1k_c^2/k_B$, and $\theta_j=\hbar c_jk_c/k_B$ for $j=$LA, TA, τ. In the low-temperature limit, we obtain from Eq. (2): $\sigma=4\times\pi^2k_B^2T/(3h)+O\left((\alpha/T)^2e^{-\alpha/T}\right)$, with $\alpha=\min\{\theta_j\}$ [31]. Therefore, at very low temperatures, the finite width graphene ribbon behaves as 4-channel thermal quantum wire with a thermal conductance $\sim T$. Notice that this is a universal, material independent limit. We remark the correspondence of this result with the low-temperature limit of the thermal conductance of a carbon nanotube [29].

In the high temperature limit, the ballistic thermal conductance depends on material specific properties through a phase-space average speed of sound $\bar{c}$ [31]:

$$\sigma/w = (3/2)k_Bn_s\bar{c} + O(w^{-2}). \quad (3)$$

If the width of the plate is very large $w\to\infty$, we notice that $c_\tau\sim 1/w\to 0$ and hence the torsion mode disappears. In this limit, we show that the thermal conductance is dominated by the bending mode at low temperatures [31],

$$\sigma/w = 0.2259k_B^{5/2}/(c_b^{1/2}\hbar^{3/2})T^{3/2}. \quad (4)$$

At intermediate temperatures, the in-plane LA and TA modes introduce a $\sim T^2$ contribution to the lattice thermal conductance. In Fig. 4, we show the thermal conductance per unit cross section of the ribbon, for different widths w, calculated from Eq. (2). We chose parameters corresponding to graphene, graphane and fluorinated graphene, respectively. As observed from Eq. (4), and in contrast with the narrow ribbon case, the infinite sheet low-temperature limit depends on material specific parameters through the bending mode coefficient $c_b=\sqrt{D/\rho_s}$.

4. Electronic structure

In this section, we turn to comparative analysis of the electronic spectra of graphene, graphane, and fluorinated graphene. Fig. 5 shows the calculated electronic band structures of a) graphene (C), b) graphane

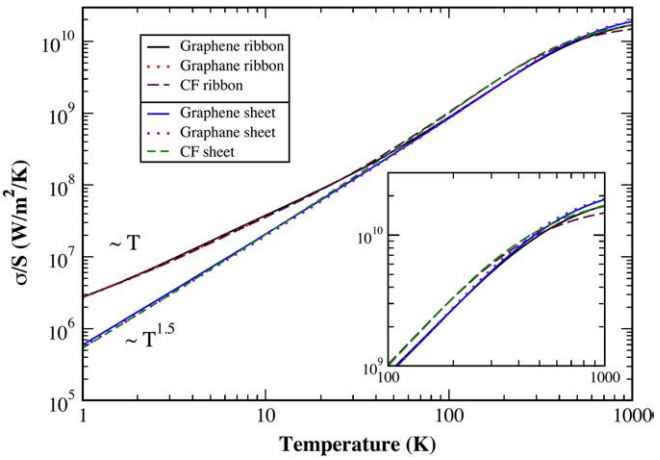

Fig. 4. Ballistic thermal conductance per unit cross section, calculated after our analytical expression (Eq. (2)), for the three different materials, graphene, graphane and fluorinated graphene (CF). We compared ribbons ($w \sim 4$ nm) and sheets ($w \to \infty$), which clearly display a distinct low-temperature dependence, in agreement with our analysis. In the inset we show a magnified view of the high temperature region.

(CH) and c) fluorinated graphene (CF). We see that carbon hydrogenation or fluorination opens a finite band gap, transforming the system into a semiconductor quite similar to sp^3 diamond. This is in contrast with graphene (Fig. 5(a)), which has a metallic behavior at a single point in reciprocal space, the K-point, were the conduction and valence bands π, π* inherited from the basic bonding and antibonding states in benzene touch. Analytical tight-binding calculations show that the dispersion for these two bands is given by the expression [32]

$$E^{\pm}(k_L, k_w) \approx \pm t\left\{1 + 4\cos\left(\sqrt{3}k_L a/2\right)\cos(k_w a/2) + 4\cos^2(k_L a/2)\right\}^{1/2}.$$

Expansion of this energy dispersion in the vicinity of the K-point $\vec{k}_F = (2\pi/(a\sqrt{3}), 2\pi/(3a))$ leads to a linear dispersion $E^{\pm} \sim \pm \hbar v_F |\vec{k} - \vec{k}_F|$, with $v_F = 10^6$ m/s. In this regime, charge carriers can be formally pictured as massless Dirac quasi-particles in the effective Hamiltonian approximation. On the other hand, as observed in Fig. 5(b), the electronic spectra of graphane (CH) and fluorinated graphene (CF) show a gap. This transition from metal to wide gap semiconductor induced by carbon hydrogenation or fluorination opens a variety of potential scenarios for applications. For example, the gap size can be tuned depending on the total concentration and spatial distribution of hydrogenated sites. Examples of this are graphene nanoroads (GNRs) [4] and quantum dots (QDs) [5], which are narrow stripes, and nanometer scale islands, respectively, of graphene carved in a hydrogenated graphane matrix. Similar structures can be conceived in a fluorinated matrix as well.

5. Interfacial designs: Nanoroads, GNR′

The design of nanodevices requires control over interfacial properties between different nanomaterials, and moreover, some of the physical principles of action of these devices may depend on these properties. Of particular interest in this context are recently synthesized graphene nanoribbons (GNR) [33–36], obtained by cutting graphene sheets and passivating the edge carbon atoms (e.g., by hydrogens). In GNRs it is possible to tune the electronic properties, by controlling the width and orientation of the edges, thus obtaining semiconducting or metallic structures [37–39]. In particular, zigzag GNRs present magnetic properties [40–43], and in the presence of an external electric field become half metallic [39,43], which makes them potential candidates for spintronic devices. Recent investigation [2,3] suggests that hydrogenation of graphene can be utilized to form geometrical areas of pristine graphene with the desired electronic properties embedded in fully hydrogenated phase, without the need for cutting [35,44]. This alternative is supported by two important features: i) A fully hydrogenated graphene is a wide gap semiconductor, and ii) it should form very sharp interfaces [2] with the pristine graphene in the same plane. A similar effect should be expected from fluorination.

By means of *ab initio* calculations, we explored the possibility of patterning the pristine graphene nanoroads (GNR′, "primed" to distinguish from similar acronym for the graphene nanoribbons GNR) via selective hydrogenation or fluorination of the graphene sheets, as depicted in Fig. 6. We show that the electronic properties of the GNRs depend sensitively upon their orientations and widths, offering the possibility of tuning for a variety of device applications.

Graphene nanoroads can be classified into armchair (AGNRs) and zigzag (ZGNRs) depending upon their number of pristine dimer lines and zigzag chains N_a and N_z, respectively, Fig. 6. Hydrogenation on both sides of a graphene sheet leads to the lowest energy structure, which corresponds to graphane. Adsorption of the first hydrogen breaks the pairing of π-electrons between two subgroups of starred and un-starred carbon atoms, leaving the system with an unpaired π-electron [45]. The radical is further removed by addition of a second hydrogen to the carbon atom from the other subgroup, thus lowering the energy. In addition, the change in carbon hybridization from sp^2 to sp^3 leads to buckling of hydrogenated carbon, and the induced strains on adjacent carbon atoms compensate each other, thus reducing the energy. A hydrogenated phase [2] with stoichiometry CH is energetically most favorable, with the distinct boundary-interface separating it from the pristine graphene area.

The relaxed geometry, studied by means of density functional theory based pseudopotential plane-wave method as implemented in VASP [16,46], differs for the two types of GNRs. The relaxed AGNRs are completely flat, Fig. 6, since alternate C atoms bonded to hydrogen move out of the plane in opposite directions along the orientation of AGNRs. On the other hand, in ZGNRs each half of the hydrogenated

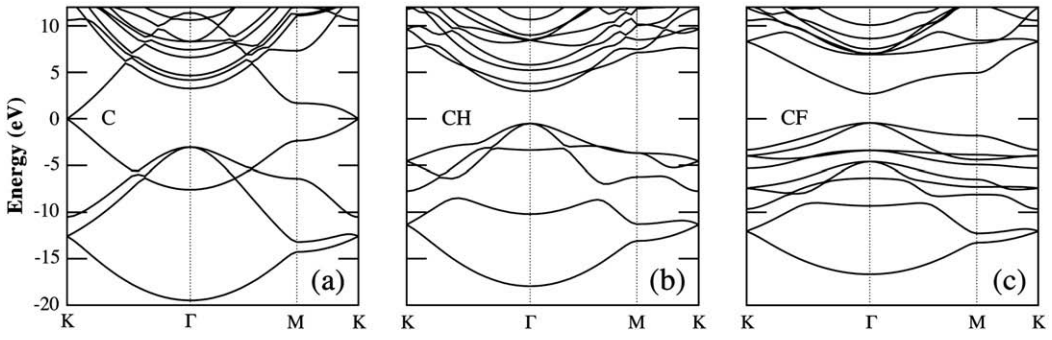

Fig. 5. The calculated band structures of: a) graphene (C), b) graphane (CH) and c) fluorinated graphene (CF). Notice that hydrogenation and fluorination in graphane and fluorinated graphene, respectively, open a band gap at the metallic K-points in graphene. The direct gaps at Γ-point are 3.48 eV and 3.12 eV for graphane and fluorinated graphene, respectively.

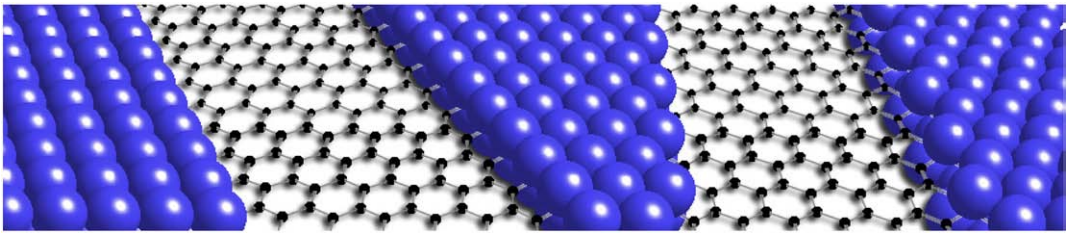

Fig. 6. Relaxed structure of zigzag (left) and armchair (right) nanoroads. The blue spheres represent Hydrogen or Fluorine. The width is measured by the number of pristine sp^2-carbon dimer-lines (N_a) or zigzag chains (N_z), respectively.

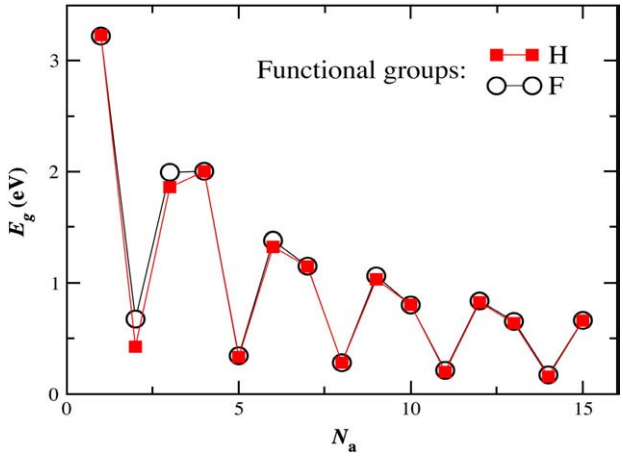

Fig. 7. The band-gap variation for nanoroads as a function of the width N_a. We compare hydrogenated AGNRs (red squares) vs fluorinated ACFNRs (open circles).

zigzag rings moves alternately in and out of the plane, introducing an overall tilt, Fig. 6. With the increasing width of the ZGNRs, the tilt becomes more localized at the interface and part of the road away from the interface remains flat. We observed that the tilt has a very little effect on electronic and magnetic properties [4]. Placing such 2D-structure on a substrate, with ever-present van der Waals attraction, should further flatten the interfacial areas. Generally, the mismatch strain along with the tilt, chemically-induced by either H or F, or oxygen groups, causes rumpling and possibly delamination of carbon-sheet from the substrates (see Fig. 1 in Ref. [44]).

We studied the electronic band structure of GNRs. The AGNRs are semiconductors, and due to quantum confinement the band gap increases when reducing their width, thus offering the possibility of tuning the band gap. Like in nanotubes and nanoribbons, the gap here becomes very small for $N_a = 3p + 2$. The variation in band gap is not monotonous and can be subdivided into three families as shown in Fig. 7. The band gaps in the three families follow hierarchy $\Delta_{3p+2} < \Delta_{3p+1} < \Delta_{3p}$ (except for the $N_a = 3$ and 4). A similar, non-monotonic trend is observed in the band gap of armchair fluorinated graphene nanoroads (ACFNRs), after calculations shown in Fig. 7. For example, the band structures from these three families for fluorinated graphene are shown in Fig. 8, essentially corroborating the trends observed in Fig. 7.

6. Conclusion

In summary, by combining first principles and tight-binding calculations with analytical methods, we presented a comprehensive characterization of three carbon nanomaterials of technological interest: graphene, graphane, and fluorinated graphene. We analyzed structural and elastic properties, confirming the high mechanical stability and in-plane stiffness of these materials. In particular, after our calculations we concluded that graphene is the most rigid among the three materials upon stretching, but the most compliant upon bending [47]. In graphane and fluorinated graphene, the sp^3 carbon hybridization induces non-planar structures. This effect, in combination with interactions between the surface CF or CH groups, translates into a higher bending stiffness and a larger effective thickness as compared with graphene. We further used our estimations of elastic parameters in an analytical model for the ballistic thermal conductance of nanoribbons, which generically represents all three materials. At low temperatures, we show a power law behavior for the thermal conductance per unit width, with an exponent β depending on the width of the ribbon. In the limit of a narrow ribbon, $\beta = 1$. We showed that in this regime, the ribbon carries exactly four quanta of thermal conductance, independent of material specific parameters. As the width of the ribbon increases, we observe a transition in the exponent towards $\beta = 1.5$ in the limit of an infinite two-dimensional sheet. In this second case, we show that the contribution from the torsion mode disappears, and heat transport at low temperatures is dominated by the bending mode, with material specific parameters. We also performed electronic structure calculations, confirming that graphene is a semi-metal. We also showed that carbon hydrogenation and fluorination opens a band gap, and in consequence graphane and fluorinated graphene are wide gap semiconductors. Finally, we

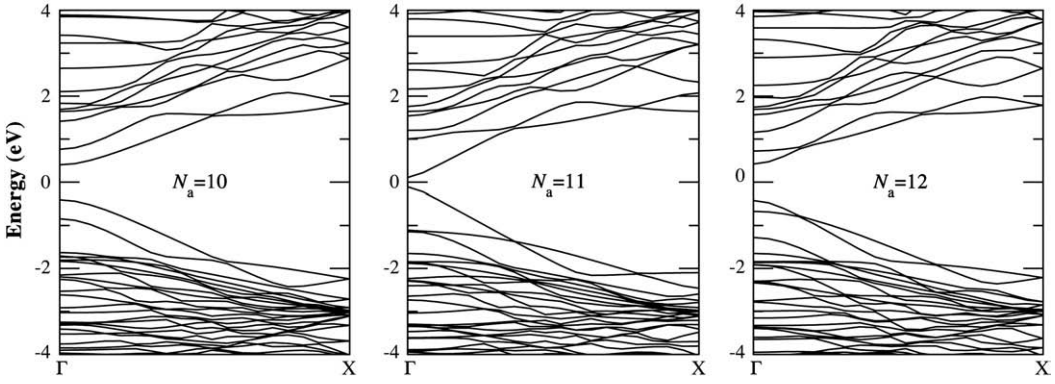

Fig. 8. The band structure for fluorinated nanoroads, at different widths $N_a = 10$, 11 and 12.

studied designed interfaces between these materials, and showed that conducting and semiconducting nanoroads can in principle be patterned on a graphene sheet by hydrogenation or fluorination. This feature, combined with the possibility of controlling band gap through geometry and orientation of the pattern, represents a promising technology for future device implementation.

Acknowledgements

This work was supported by the National Science Foundation (CMMI) and by the Office of Naval Research, with E.M. partially supported within the LANCER project by the Lockheed Martin Corporation. M.A.R. is a Roberto Rocca Fellowship recipient.

References

[1] A.K. Singh, M.A. Ribas, B.I. Yakobson, ACS Nano 3 (2009) 1657.
[2] Y. Lin, F. Ding, B.I. Yakobson, Phys. Rev. B 78 (2008) 041402.
[3] J.O. Sofo, A.Y. Chaudhari, G.D. Barber, Phys. Rev. B 75 (2007) 153401.
[4] A.K. Singh, B.I. Yakobson, Nano Lett. 8 (2009) 1540.
[5] A.K. Singh, E.S. Penev, B.I. Yakobson, (Submitted), (2009).
[6] K.S. Novoselov, D. Jiang, F. Schedin, T.J. Booth, V.V. Khotkevich, S.V. Morozov, A.K. Geim, Proc. Natl. Acad. Sci. 102 (2005) 10451.
[7] K.S. Novoselov, A.K. Geim, S.V. Morozov, D. Jiang, Y. Zhang, S.V. Dubonos, I.V. Grigorieva, A.A. Firsov, Science 306 (2004) 666.
[8] A.K. Geim, K.S. Novoselov, Nature Mater. 6 (2007) 182.
[9] T.J. Booth, P. Blake, R. Nair, D. Jiang, E.W. Hill, U. Bangert, A. Blecloch, M. Gass, K.S. Novoselov, M.I. Katsnelson, A.K. Geim, Nano Lett. 8 (2008) 2442.
[10] W. Rudorff, G. Rudorff, Z. Anorg. Allg. Chem. 253 (1947) 281.
[11] T. Mallouk, N. Bartlett, J. Chem. Soc., Chem. Commun. (1983) 103.
[12] W. Rudorff, G. Rudorff, Chem. Ber. 80 (1947) 417.
[13] K.N. Kudin, G.E. Scuseria, B.I. Yakobson, Phys. Rev. B 64 (2001) 235406.
[14] B.I. Yakobson, C.J. Brabec, J. Bernholc, Phys. Rev. Lett. 76 (1996) 2511.
[15] J. Tersoff, R.S. Ruoff, Phys. Rev. Lett. 73 (1994) 676.
[16] G. Kresse, J. Furthmüller, Phys. Rev. B 54 (1996) 11169.
[17] G. Kresse, J. Hafner, Phys. Rev. B 47 (1993) 558.
[18] G. Kresse, J. Hafner, J. Phys.: Condens. Matter 6 (1994) 8245.
[19] G. Kresse, J. Hafner, Phys. Rev. B 49 (1994) 14251.
[20] G. Kresse, D. Joubert, Phys. Rev. B 59 (1999) 1758.
[21] J.P. Perdew, K. Burke, M. Ernzerhof, Phys. Rev. Lett. 77 (1996) 3865.
[22] B. Aradi, B. Hourahine, T. Frauenheim, J. Phys. Chem. A 111 (2007) 5678.
[23] M. Elstner, D. Porezag, G. Jungnickel, J. Elsner, M. Haugk, T. Frauenheim, S. Suhai, G. Seifert, Phys. Rev. B 58 (1998) 7260.
[24] N.C. Craig, A. Chen, K.H. Suh, S. Klee, G.C. Mellau, B.P. Winnewisser, M. Winnewisser, J. Am. Chem. Soc. 119 (1997) 4789.
[25] S. Berber, Y.-K. Kwon, D. Tománek, Phys. Rev. Lett. 84 (2000) 4613.
[26] M.A. Osman, D. Srivastava, Nanotechnology 12 (2001) 21.
[27] S. Ghosh, I. Calizo, D. Teweldebrhan, E.P. Pokatilov, D.L. Nika, A.A. Balandin, W. Bao, F. Miao, C.N. Lau, Appl. Phys. Lett. 92 (2008) 151911.
[28] S.P. Hepplestone, G.P. Srivastava, J. Phys. Conf. Ser. 92 (2007) 012076.
[29] N. Mingo, D.A. Broido, Phys. Rev. Lett. 95 (2005) 096105.
[30] R. Saito, J. Nakamura, A. Natori, Phys. Rev. B 76 (2007) 115409.
[31] E. Muñoz, B.I. Yakobson, (Unpublished results), (2009).
[32] R. Saito, G. Dresselhaus, M.S. Dresselhaus, Physical Properties of Carbon Nanotubes, Imperial College Press, London, 1998.
[33] M. Han, B. Ozyilmaz, Y. Zhang, P. Kim, Phys. Rev. Lett. 98 (2007) 206805.
[34] C. Berger, Z. Song, X. Li, X. Wu, N. Brown, C.C. Naud, D. Mayou, T. Li, J. Hass, A.N. Marchenkov, E.H. Conrad, P.N. First, W.A.D. Heer, Science 312 (2006) 1191.
[35] L. Ci, Z. Xu, L. Wang, W. Gao, F. Ding, K. Kelly, B. Yakobson, P. Ajayan, Nano Research 1 (2008) 116.
[36] Z. Chen, Y. Lin, M.J. Rooks, P. Avouris, Physica E 40 (2007) 228.
[37] M. Ezawa, Phys. Rev. B 73 (2006) 045432.
[38] L.G. Cancado, M.A. Pimenta, B.R.A. Neves, G. Medeiros-Ribeiro, T. Enoki, Y. Kobayashi, K. Takai, K.-I. Fukui, M.S. Dresselhaus, R. Saito, A. Jorio, Phys. Rev. Lett. 93 (2004) 047403.
[39] Y. Son, M. Cohen, S. Louie, Nature 444 (2006) 347.
[40] M. Fujita, K. Wakabayashi, K. Nakada, K. Kusakabe, J. Phys. Soc. Jpn. 65 (1996) 1920.
[41] K. Wakabayashi, M. Fujita, H. Ajiki, M. Sigrist, Phys. Rev. B 59 (1999) 8271.
[42] K.N. Kudin, B. Ozbas, H.C. Schniepp, R.K. Prud'homme, I.A. Aksay, R. Car, Nano Lett. 8 (2008) 36.
[43] O. Hod, V. Barone, J. Peralta, G. Scuseria, Nano Lett. 7 (2007) 2295.
[44] P.M. Ajayan, B.I. Yakobson, Nature 441 (2006) 818.
[45] M.J.S. Dewar, R.C. Dougherty, The PMO Theory of Organic Chemistry, Plenum, New York, 1975.
[46] G. Kresse, J. Furthmüller, Comput. Mat. Sci. 6 (1996) 15.
[47] K.V. Bets, B.I. Yakobson, Nano Res. 2 (2009) 161.